https://doi.org/10.5194/egusphere-2026-2784
Preprint. Discussion started: 1 June 2026

Westward extension of ENSO teleconnections links spring rainfall between northern Southeast Asia and the Arabian Peninsula

Dzung Nguyen–Le[1]*

[1] Department of Space and Earth Sciences, University of Science and Technology of Hanoi (USTH), Vietnam Academy of Science and Technology (VAST), Hanoi, Vietnam

* *Corresponding author:* Dzung Nguyen–Le (Email: nguyen-le.dung@usth.edu.vn; ORCID: 0000-0003-0214-3411)

Abstract. ENSO teleconnections are not stationary, but how this nonstationarity reorganizes spring hydroclimate across Asia remains unclear. Spring rainfall is particularly important for the Arabian Peninsula, one of the world's most arid regions, where even modest rainfall changes can affect water availability and drought risk. Here we show that a March–April rainfall seesaw between the Arabian Peninsula and northern Southeast Asia strengthened markedly after the late 1990s. During 1979–1998, ENSO-related convection and circulation anomalies remained mainly confined to the tropical Pacific–Maritime Continent sector and projected only weakly toward the Arabian Peninsula, with limited evidence of a coherent pathway linking the two regions. During 1999–2023, the ENSO-related response extended farther westward and northwestward, linking El Niño-related suppressed convection and reduced rainfall over northern Southeast Asia with enhanced rainfall over the Arabian Peninsula. This shift was associated with a reorganization of Indo-Pacific overturning, including a more distinct double-cell Walker response, a strengthened Arabian Peninsula vertical branch extending farther northward, and enhanced upper-level Rossby-type and thermal adjustment. Idealized model experiments show that western equatorial Indian Ocean heating can generate an Arabian Peninsula-sector response and that this response becomes more effective under the later-period background state. Observed changes in convection, low-level pressure and winds, and the upper-level jet and divergence further indicate that the later-period ENSO anomalies developed

https://doi.org/10.5194/egusphere-2026-2784
Preprint. Discussion started: 1 June 2026

within a modified mean-state environment. These results identify a nonstationary ENSO teleconnection pathway in which the westward extension of tropical heating anomalies, Walker–Hadley coupling, and off-equatorial upper-level adjustment connect spring rainfall variability across Southeast and West Asia.

1. Introduction

Spring rainfall during March–April plays a critical role in hydroclimate variability across West and Southeast Asia. Over the Arabian Peninsula (AP), rainfall is generally sparse and highly variable, but spring precipitation contributes a substantial fraction of the annual total, reaching 50% in some southern areas (Fig. S1). Because the AP lies within one of the world's most arid regions, even modest changes in spring rainfall can affect drought risk, dust activity, groundwater recharge, vegetation conditions, and water-resource availability (Peel et al., 2007; Barlow et al., 2016; Almazroui et al., 2019). AP spring rainfall variability is also linked to circulation anomalies involving the subtropical westerlies, the Mediterranean–Middle East storm track, the Indian Ocean, and tropical–extratropical wave activity (Rodwell and Hoskins, 1996; Kang et al., 2015; Barlow et al., 2016).

Over northern Southeast Asia (SEA), boreal spring marks the transition from the dry winter monsoon to the wet summer monsoon regime. Rainfall during this period regulates soil moisture before monsoon onset and strongly affects agriculture, water resources, and ecosystem productivity (Chang et al., 2005; LinHo et al., 2008). Deficits in pre-monsoon rainfall can intensify heat stress, drought, and wildfire risk, whereas anomalously wet conditions can alter land–atmosphere feedbacks before the rainy season begins (Kiguchi et al., 2016). Although the AP and northern SEA are geographically distant and climatologically distinct, both regions are embedded within the broader Indo-Pacific climate system. This raises the possibility that their spring rainfall variability may become dynamically linked under certain large-scale circulation states.

https://doi.org/10.5194/egusphere-2026-2784
Preprint. Discussion started: 1 June 2026

The El Niño–Southern Oscillation (ENSO) is the dominant mode of interannual climate variability and exerts widespread influence across the Indo-Pacific (Rasmusson and Carpenter, 1982; Wang et al., 2000; Trenberth et al., 2002; McPhaden et al., 2006). ENSO-related sea surface temperature (SST) anomalies modify deep convection over the tropical Pacific, reorganize the Walker circulation, and excite atmospheric responses that extend into the subtropics and extratropics (Hoskins and Karoly, 1981; Sardeshmukh and Hoskins, 1988; Alexander et al., 2002). During boreal spring, El Niño events are typically associated with suppressed convection and reduced rainfall over northern SEA, whereas La Niña tends to enhance rainfall (Wang et al., 2000; Juneng and Tangang, 2005; Räsänen et al., 2016; Nguyen-Thanh et al., 2023; Nguyen-Le, 2024). Over the AP, ENSO influences are generally weaker and more indirect, often mediated by the Indian Ocean, subtropical westerlies, tropical–extratropical wave activity, and intraseasonal variability (Rodwell and Hoskins, 1996; Ashok et al., 2007; Kang et al., 2015; Barlow et al., 2016; Almazroui et al., 2022; Almazroui, 2023; Horan et al., 2023; Zheng and Hoteit, 2025). Despite extensive documentation of ENSO impacts on each region separately, it remains unclear whether ENSO can dynamically connect spring rainfall variability between northern SEA and the AP.

A key challenge is that ENSO teleconnections are not stationary. Their amplitude, spatial pattern, and regional expression can vary across decades because of changes in ENSO diversity, tropical mean-state conditions, Indo-Pacific SST gradients, and extratropical waveguide structure (Power et al., 1999; Deser et al., 2004; Yeh et al., 2009; Cai et al., 2014; Xie et al., 2016; Wang et al., 2020). The late 1990s marked a prominent transition in Pacific decadal variability and coincided with accelerated warming of the Indian Ocean (Dong and McPhaden, 2017; Hu et al., 2020). Since the early 2000s, ENSO characteristics have also shifted, including changes in the relative occurrence of central-Pacific, or ENSO Modoki-like, El Niño events and the decay behavior of canonical El Niño episodes (Lübbecke and McPhaden, 2014; Rodrigues et al., 2019; Hu et al., 2020). These changes can alter tropical convection, the Walker circulation, upper-tropospheric zonal winds, and

https://doi.org/10.5194/egusphere-2026-2784
Preprint. Discussion started: 1 June 2026

Rossby-wave propagation pathways. Previous studies have documented decadal changes in ENSO properties, tropical Pacific variability, and Indo-western Pacific teleconnection pathways, including changes in how ENSO-related anomalies project onto Asian hydroclimate (Hu et al., 2013; Wang et al., 2013; Wang et al., 2020; Dong and McPhaden, 2017; Hu et al., 2020). Whether such nonstationarity has reorganized rainfall coherence between distant Asian regions such as northern SEA and the AP has not been systematically examined.

The potential SEA–AP connection is physically meaningful because the two regions lie on different sides of the Indo-Pacific overturning system. Northern SEA is located near the Maritime Continent and western Pacific, where ENSO strongly modulates deep convection and the Walker circulation. The AP lies farther west and poleward, where ENSO signals must be transmitted through tropical overturning, regional meridional circulation, subtropical wave activity, and background-flow influences. A strengthened AP–SEA rainfall relationship would therefore indicate more than a local rainfall correlation; it would point to a broader reorganization of the Indo-Pacific teleconnection pathway. In particular, a westward and northwestward extension of ENSO-related circulation anomalies could link convection anomalies over northern SEA with opposite rainfall anomalies over the AP through coupled Walker–Hadley adjustment and upper-level Rossby-type responses.

In this study, we examine how the March–April rainfall relationship between northern SEA and the AP has changed since the late 1990s and how this change is linked to ENSO teleconnection variability. We first document the emergence of an anti-phase rainfall relationship between the two regions and evaluate its dependence on Niño3.4 and Indian Ocean basin-wide SST variability. We then diagnose associated changes in tropical convection, lower- and upper-level circulation, Walker–Hadley overturning, and upper-level Rossby-type and thermal responses. Finally, we examine March–April mean-state changes and perform idealized model experiments with prescribed western equatorial Indian Ocean heating to test whether this heating can generate an AP-sector response and whether that response depends on the background state. Our analysis shows that the strengthened

https://doi.org/10.5194/egusphere-2026-2784
Preprint. Discussion started: 1 June 2026

SEA–AP rainfall linkage reflects a nonstationary ENSO teleconnection pathway involving reorganized Indo-Pacific overturning, off-equatorial upper-level adjustment, and a background-state-sensitive response to western Indian Ocean heating.

2. Data and methods

2.1 Observational and reanalysis datasets

This study focuses on March–April (MA) during 1979–2023. Monthly atmospheric fields were obtained from the European Centre for Medium-Range Weather Forecasts (ECMWF) ERA5 reanalysis (Hersbach et al., 2020). The variables used include horizontal winds, vertical velocity, geopotential height, air temperature, velocity potential, divergent winds, mean sea-level pressure, and upper-level divergence. ERA5 fields were analyzed at a horizontal resolution of 0.25° × 0.25° unless otherwise stated. Monthly sea surface temperature (SST) anomalies were obtained from the Hadley Centre Sea Ice and Sea Surface Temperature dataset (HadISST; Rayner et al., 2003), available on a 1° × 1° grid. Monthly precipitation data were taken from the CMAP with a horizontal resolution of 2.5° × 2.5° and available from 1979 to the present (Xie and Arkin, 1997). The Global Precipitation Climatology Project (GPCP; Adler et al., 2003) v2.3 dataset is used to verify the robustness of the CMAP-based findings. Outgoing longwave radiation (OLR), used as a proxy for deep tropical convection, was obtained from the NOAA Climate Data Record (CDR) on a 2.5° × 2.5° grid (Lee et al., 2007). All variables were converted to March–April seasonal means for each year. Monthly anomalies were calculated by subtracting the 1979–2023 climatological mean, and linear trends were removed.

2.2 Rainfall, SST, Walker circulation, and vertical-branch indices

The Arabian Peninsula (AP) rainfall index was defined as the area-averaged March–April precipitation over 12.5°–32.5°N, 35°–60°E. The northern Southeast Asia (SEA) rainfall index was defined as the area-averaged March–April precipitation over 0°–20°N, 90°–130°E. Area averages

https://doi.org/10.5194/egusphere-2026-2784
Preprint. Discussion started: 1 June 2026

were weighted by the cosine of latitude. ENSO variability was represented by the Niño3.4 index, calculated as the normalized SST anomalies averaged over 5°S–5°N, 170°–120°W. The Indian Ocean Basin Mode index (IOBMI; Yang et al., 2007; 2009) was calculated as the area-averaged SST anomalies over 20°S–20°N, 40°–110°E. Both indices were calculated for March–April and standardized over 1979–2023. The analysis period was divided into an earlier period, P1 (1979–1998), and a later period, P2 (1999–2023), based on the late-1990s transition indicated by the moving-correlation diagnostics.

The Walker circulation index (WCI) was defined using the sea-level pressure difference between the eastern and western tropical Pacific (Vecchi et al., 2006). First, the raw *dSLP* index is calculated as the sea-level pressure anomaly difference between the eastern tropical Pacific (5°S–5°N, 160°–80°W) and the western tropical Pacific (5°S–5°N, 80°–160°E):

$$dSLP = \langle \mathrm{SLP}' \rangle_{5°\mathrm{S}-5°\mathrm{N},\,160°-80°\mathrm{W}} - \langle \mathrm{SLP}' \rangle_{5°\mathrm{S}-5°\mathrm{N},\,80°-160°\mathrm{E}} \quad (1)$$

where SLP′ denotes the March–April sea-level pressure anomaly, and angle brackets denote area averaging. Because this raw *dSLP* index tends to be negative during El Niño conditions, we define:

$$\mathrm{WCI} = -\mathrm{dSLP}. \quad (2)$$

With this sign convention, positive WCI values correspond to an El Niño-like weakening of the Pacific Walker pressure gradient. This index is used to quantify the large-scale Pacific Walker circulation variability associated with ENSO.

Regional vertical-branch indices (VBI) were defined using the layer-mean pressure velocity over 700–300 hPa. Because upward motion corresponds to negative pressure velocity, the VBI was calculated from -ω:

$$\mathrm{VBI} = \langle -\omega \rangle_{700-300\ \mathrm{hPa}}. \quad (3)$$

Positive VBI values therefore indicate stronger upward motion. The AP VBI was averaged over 12.5°–32.5°N, 35°–60°E, and the SEA VBI was averaged over 0°–20°N, 90°–130°E.

https://doi.org/10.5194/egusphere-2026-2784
Preprint. Discussion started: 1 June 2026

2.3 Regression, partial correlation, and moving correlation analyses

Linear regression was used to quantify the atmospheric response to ENSO. For each period, March–April atmospheric anomalies were regressed onto the standardized Niño3.4 index. Differences in regression coefficients were calculated as P2 minus P1.

To remove the respective impacts of IOBM and Niño-3.4 indices, we employ a partial correlation method (Ashok et al., 2007; Whittaker, 2008). The partial correlation coefficient is calculated as:

$$r_{12|3} = \frac{r_{12} - r_{13}r_{23}}{\sqrt{1-r_{13}^2}\sqrt{1-r_{23}^2}} \quad (4)$$

where r_{ij} represents the linear correlation coefficient between variables A_i and A_j, and $r_{12|3}$ denotes the partial correlation coefficient between A_1 and A_2 after removing the influence of A_3.

Time-varying relationships were examined using 19-year moving correlations. The statistical significance of correlation coefficients is assessed using a two-tailed Student's t-test, accounting for the effective number of degrees of freedom N_{eff} (Bretherton et al., 1999). Unless otherwise stated, all significance is evaluated at the 95% confidence level. N_{eff} is calculated based on the lag–1 autocorrelation of variables x and y as:

$$N_{eff} = N\frac{1-r_x r_y}{1+r_x r_y} \quad (5)$$

where N is the original sample size, and r_1 and r_2 are the lag–1 autocorrelation coefficient of variables x and y, respectively.

2.4 Wave activity flux and Rossby wave source diagnostics

The stationary wave activity flux (WAF; Takaya and Nakamura, 2001) was calculated to diagnose the preferred direction of Rossby wave activity propagation. WAF vectors were masked in the deep tropics and in regions of weak background flow and were scaled for display. They are interpreted qualitatively as indicators of the stationary wave-activity pathway.

https://doi.org/10.5194/egusphere-2026-2784
Preprint. Discussion started: 1 June 2026

$$F = \frac{p\cos\phi}{2|U|}\begin{Bmatrix} \frac{U}{a^2\cos^2\phi}\left[\left(\frac{\partial\psi'}{\partial\lambda}\right)^2 - \psi'\frac{\partial^2\psi'}{\partial\lambda^2}\right] + \frac{V}{a^2\cos\phi}\left(\frac{\partial\psi'}{\partial\lambda}\frac{\partial\psi'}{\partial\phi} - \psi'\frac{\partial^2\psi'}{\partial\lambda\,\partial\phi}\right) \\ \frac{U}{a^2\cos\phi}\left(\frac{\partial\psi'}{\partial\lambda}\frac{\partial\psi'}{\partial\phi} - \psi'\frac{\partial^2\psi'}{\partial\lambda\,\partial\phi}\right) + \frac{V}{a^2}\left[\left(\frac{\partial\psi'}{\partial\phi}\right)^2 - \psi'\frac{\partial^2\psi'}{\partial\phi^2}\right] \end{Bmatrix} \quad (6)$$

where p denotes the pressure normalized by 1000 hPa, a is Earth's radius, φ is the latitude, λ is the longitude, and $|U|$, U, and V represent the basic states of wind speed, and the zonal and meridional wind components, respectively. The perturbation streamfunction ψ' was calculated from 200-hPa geopotential height as

$$\psi' = \frac{gZ'_{200}}{f}, \quad (7)$$

where g is gravitational acceleration and $f = 2\Omega\sin\varphi$ is the Coriolis parameter, with Ω representing the Earth's rotation rate. WAF vectors were masked in the deep tropics and in regions of weak background flow and were scaled for display. They are interpreted qualitatively as indicators of the preferred stationary wave-activity pathway.

The Rossby wave source (RWS) is a term used to describe the mechanisms that generate and maintain Rossby waves. It was calculated from the divergent wind and absolute vorticity fields (Sardeshmukh and Hoskins, 1998).

$$S = -\nabla\left(\vec{V_\chi}\zeta_a\right) = -fD_\chi - \zeta D_\chi - \vec{V_\chi}\cdot\nabla(f+\zeta) \quad (8)$$

where S is the source/sink of the Rossby wave; $\vec{V_\chi}$ denotes the divergent wind vector, ζ_a is the absolute vorticity, f and ζ are the planetary vorticity and relative vorticity, respectively, and D_χ is the horizontal divergence.

2.5 Idealized model experiments

A global primitive equation model called DREAM (Dynamical Research Empirical Atmospheric Model; Hall, 2000) is employed to analyze the response of the atmospheric circulation to diabatic heating released by precipitation anomalies. The version used here is the latest release (v8.4; Hall and Leroux, 2023; Leroux and Hall, 2025). Previous studies have applied DREAM to examine the

https://doi.org/10.5194/egusphere-2026-2784
Preprint. Discussion started: 1 June 2026

extratropical atmospheric response to prescribed tropical forcings, such as ENSO-related heating (Hall and Derome, 2000; Lin et al., 2007).

A set of idealized experiments is conducted using the DREAM model to examine whether heating over the western equatorial Indian Ocean can generate an AP-sector circulation response, and whether this response depends on the March–April background state. The prescribed heating is centered over the western equatorial Indian Ocean at 60°E, 0°N, corresponding to the observed later-period ENSO-related convective/heating anomalies on the western side of the Indo-Pacific overturning system. Two experiments are performed with the same heating perturbation but different basic states: one using the March–April climatological background for P1 (1979–1998), and the other using the March–April climatological background for P2 (1999–2023). This design isolates the sensitivity of the forced response to the changed background circulation while keeping the imposed heating identical.

All experiments are performed at T42 horizontal resolution with 15 vertical levels on σ surfaces. The basic states are derived from ERA5 March–April climatologies for the corresponding periods and are used to initialize the model and construct the forcing environment. Each integration is run for 20 days, and the atmospheric responses averaged over days 11–20 are analyzed. The heating perturbation is imposed in the thermodynamic equation, switched on at the initial time, and maintained throughout the integration. No forcing is applied to the vorticity, divergence, or mass equations.

The imposed heating represents an idealized diabatic heating anomaly associated with enhanced convection over the western equatorial Indian Ocean (Fig. S2). The imposed heating has an elliptical horizontal structure with semimajor and semiminor axes of 20° longitude and 12.5° latitude, respectively (Hall and Derome, 2000; Lin et al., 2007). Its amplitude follows a squared-cosine distribution with distance from the heating center. The vertical profile is prescribed as

$$Q(\sigma) = Q_0 \pi (1-\sigma)\, sin[\pi(1-\sigma)] \tag{9}$$

https://doi.org/10.5194/egusphere-2026-2784
Preprint. Discussion started: 1 June 2026

where $\sigma = p/p_0$, p is the pressure and p_0 = 1000 hPa. The continuous profile peaks near $\sigma \cong 0.35$; on the 15-level DREAM grid, $\sigma = 0.4$ (~400 hPa) is used as a representative maximum-heating level. The vertically averaged heating rate at the center, Q_0 is 1 K day^{-1}, approximately equivalent to latent heating associated with a precipitation rate of about 4 mm day^{-1}.

2.6 Statistical significance

The statistical significance of differences between the two periods was assessed using bootstrap resampling (Storch and Zwiers, 1999). For mean-state differences, years were resampled with replacement within P1 and P2, and the P2–P1 mean difference was recalculated. For regression differences, years were resampled with replacement within each period, regression coefficients onto Niño3.4 were recomputed, and the P2–P1 regression difference was recalculated. This procedure was repeated 2000 times to construct a bootstrap distribution. Differences were considered significant at the 95% confidence level when the bootstrap distribution indicated that the sign of the observed difference was unlikely to arise by chance.

3. Emergence of an ENSO-dependent SEA–AP rainfall seesaw

Spring rainfall over the AP and northern SEA shows a marked change after the late 1990s. The 19-year moving correlation between March–April rainfall anomalies in the two regions is weak and statistically insignificant during the earlier part of the record but becomes strongly negative after the late 1990s (Fig. 1a). This anti-phase relationship indicates that wetter-than-normal spring conditions over the AP tend to coincide with drier-than-normal conditions over northern SEA, and vice versa, during the later period.

The rainfall seesaw is closely tied to ENSO variability. Removing Niño3.4 substantially weakens the post-1990s negative correlation, whereas removing the IOBM produces a smaller reduction (Fig. 1a). This contrast indicates that the recent SEA–AP rainfall seesaw is primarily associated with ENSO rather than Indian Ocean basin-wide SST variability alone. Similar behavior

https://doi.org/10.5194/egusphere-2026-2784
Preprint. Discussion started: 1 June 2026

241 is obtained using 17-year and 21-year moving correlations and the GPCP rainfall dataset, suggesting
242 that the result is not sensitive to the moving-window length or precipitation dataset.

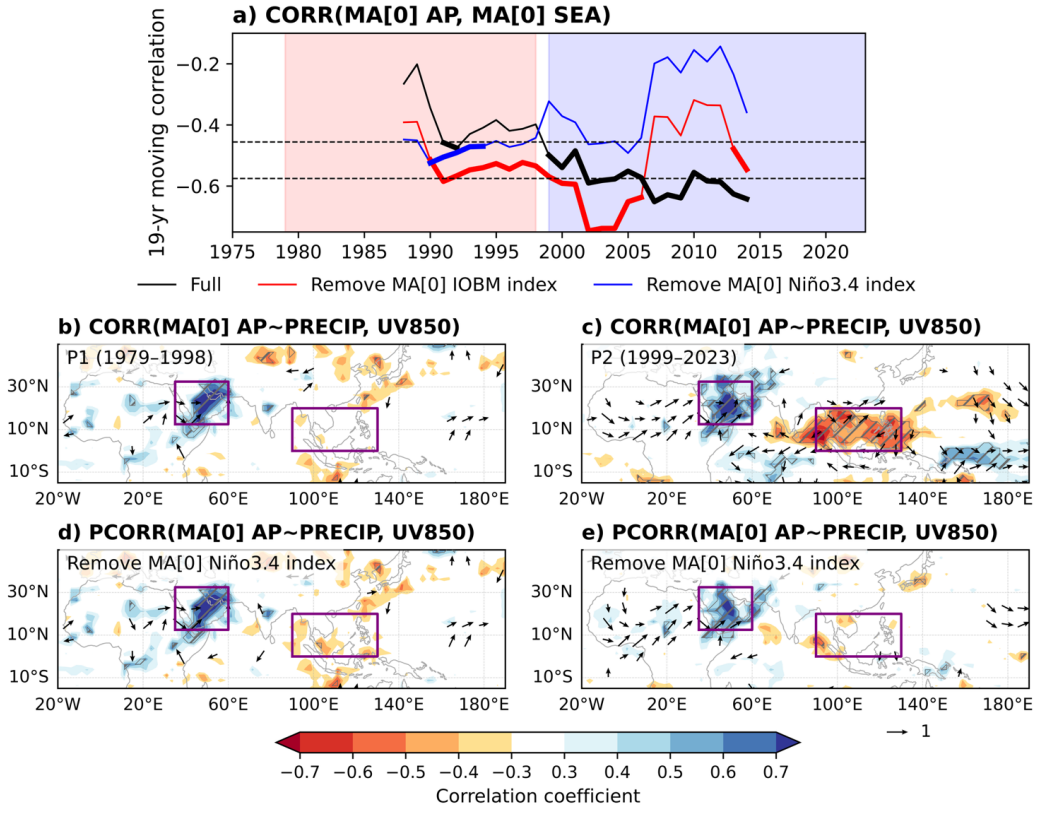

243

244 **Figure 1:** Emergence of a spring rainfall seesaw between the Arabian Peninsula and northern Southeast Asia
245 and its ENSO dependence. (a) Nineteen-year moving correlation between March–April rainfall anomalies
246 over the Arabian Peninsula (AP) and northern Southeast Asia (SEA) during 1979–2023. The black line shows
247 the raw correlation. The red and blue lines show the corresponding correlations after removing the March–
248 April Indian Ocean Basin Mode (IOBM) index and Niño3.4 index, respectively. Thick line segments indicate
249 statistically significant correlations, and dashed horizontal lines denote the 95 % and 99 % confidence levels.
250 Red and blue shading mark the earlier period P1 (1979–1998) and later period P2 (1999–2023), respectively.
251 (b,c) Correlations of March–April rainfall anomalies (shading) and 850-hPa winds (vectors) with AP rainfall
252 during (b) P1 and (c) P2. (d,e) As in (b,c), but after removing Niño3.4 variability. Hatching denotes
253 statistically significant rainfall correlations, and only significant wind vectors are shown. Purple boxes
254 indicate the AP and SEA regions.

https://doi.org/10.5194/egusphere-2026-2784
Preprint. Discussion started: 1 June 2026

Spatial correlation maps further show that the AP rainfall association with Indo-Pacific rainfall and low-level circulation changes substantially between the two periods. During P1, AP rainfall is only weakly related to northern SEA rainfall and the surrounding 850-hPa circulation (Fig. 1b). During P2, however, AP rainfall is associated with a clearer Indo-Pacific circulation pattern, including anomalous low-level flow and an opposite rainfall signal over northern SEA (Fig. 1c). After Niño3.4 variability is removed, this organized AP–SEA rainfall and circulation pattern is substantially weakened (Fig. 1e), indicating that ENSO is the principal large-scale factor in the later-period seesaw.

This result is not limited to the AP-reference perspective. When northern SEA rainfall is used as the reference index, the later-period correlation pattern also shows a clearer connection with AP rainfall and Indo-Pacific low-level circulation, and this connection weakens after removing Niño3.4 variability (Fig. S3). These results indicate that the SEA–AP spring rainfall seesaw emerged as part of an intensified and spatially reorganized ENSO teleconnection after the late 1990s. The regional importance of March–April rainfall is further supported by the climatological rainfall and seasonal rainfall-fraction analysis (Fig. S1). The following sections examine the circulation pathway associated with this change.

4. Physical mechanisms underlying the ENSO-dependent SEA–AP rainfall seesaw

4.1 Reorganization of ENSO-related lower- and upper-level circulation

To identify the large-scale circulation pathway associated with the emerging rainfall seesaw, we compare the March–April ENSO-related lower- and upper-level responses between P1 and P2. During P1, the ENSO-regressed OLR anomalies are mainly organized along the equatorial Indo-Pacific, with suppressed convection over the Maritime Continent/western Pacific and enhanced convection farther east (Fig. 2a). The associated 850-hPa wind response is also largely confined to the tropical Indo-Pacific, indicating a primarily equatorial Walker-circulation adjustment.

https://doi.org/10.5194/egusphere-2026-2784
Preprint. Discussion started: 1 June 2026

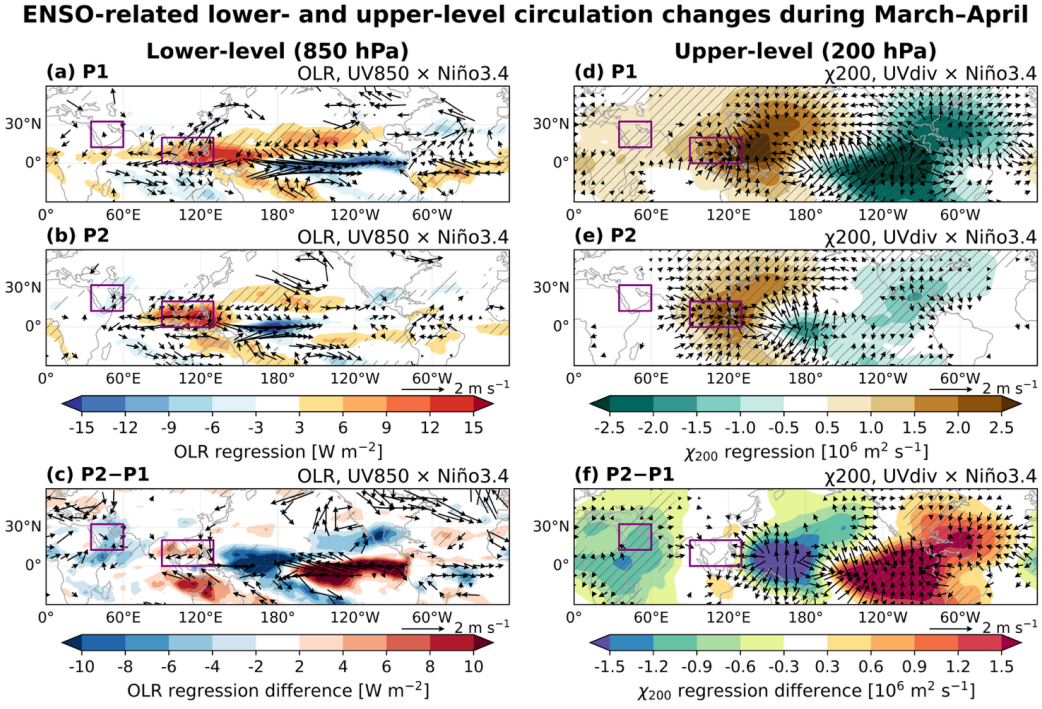

Figure 2: ENSO-related lower- and upper-level circulation changes during March–April. (a,b) Regression of OLR anomalies (shading; W m-2) and 850-hPa wind anomalies (vectors; m s-1) onto the standardized March–April Niño3.4 index during (a) P1 (1979–1998) and (b) P2 (1999–2023). (c) Difference in regression coefficients between P2 and P1 for OLR and 850-hPa winds. (d,e) As in (a,b), but for 200-hPa velocity potential χ200 anomalies (shading; 106 m2 s-1) and 200-hPa divergent wind anomalies (vectors; m s-1). (f) Difference in upper-level regression coefficients between P2 and P1. Hatching indicates statistically significant shading anomalies, and only significant wind vectors are plotted. Purple boxes indicate the Arabian Peninsula (AP), northern Southeast Asia (SEA), and Niño3.4 regions.

During P2, the lower-level ENSO response becomes more spatially organized and extends farther westward and northwestward (Fig. 2b). The later-period convective response also becomes more concentrated toward the equatorial central Pacific, giving the pattern a more central-Pacific-weighted, ENSO Modoki-like structure (Ashok et al., 2007; Nguyen-Thanh et al., 2023). Such a configuration is dynamically relevant because different ENSO SST anomaly patterns can shift the

https://doi.org/10.5194/egusphere-2026-2784
Preprint. Discussion started: 1 June 2026

Walker circulation and modify the Philippine Sea circulation response, including the occurrence and strength of anomalous circulation over the Philippine Sea (Ashok et al., 2007; Nguyen-Le et al., 2024). Consistent with this structure, the OLR and 850-hPa wind regressions show a clearer connection among the tropical Indo-Pacific, northern SEA, the western North Pacific, and the AP sector. The P2–P1 difference further highlights this reorganization, with convection and low-level circulation anomalies extending from the Maritime Continent/western Pacific toward the tropical–subtropical Indo-Pacific and AP-side sector (Fig. 2c).

The anomalous circulation over the western North Pacific is consistent with the well-established Pacific–East Asian teleconnection: during El Niño, suppressed convection over the Maritime Continent/western Pacific can excite an anomalous anticyclonic response over the western North Pacific/Philippine Sea, providing a bridge between tropical Pacific forcing and East Asian climate anomalies (Wang et al., 2000; Xie et al., 2016; Li et al., 2017). In the present case, this canonical response is more clearly expressed during P2 and is accompanied by a broader westward extension toward the western Indian Ocean and AP sector.

The upper-level divergent circulation also shows a marked reorganization. During P1, the 200-hPa velocity-potential response is broad, with positive χ_{200} anomalies extending across much of West Asia and the Indo-Pacific sector (Fig. 2d). During P2, the positive χ_{200} response becomes more confined toward East Asia and the western North Pacific, while the divergent-wind anomalies over the tropical Indo-Pacific become more coherent (Fig. 2e). Consequently, the P2–P1 difference shows significant negative χ_{200} anomalies over West Asia and positive anomalies farther east (Fig. 2f), indicating a redistribution of upper-level divergent circulation rather than a simple expansion of the P1 pattern. This redistribution is consistent with a changed Walker-circulation structure and provides the divergent-flow background for the Walker–Hadley and Rossby-type responses examined below.

These diagnostics indicate that the post-1990s rainfall linkage is associated with a spatially reorganized ENSO circulation response. At low levels, the OLR and 850-hPa wind anomalies show a

https://doi.org/10.5194/egusphere-2026-2784
Preprint. Discussion started: 1 June 2026

clearer connection from the tropical Indo-Pacific toward northern SEA and the AP sector. At upper levels, the velocity-potential and divergent-wind fields indicate a redistribution of divergent circulation, with reduced positive χ_{200} anomalies over West Asia and enhanced anomalies farther east. Together, these changes suggest that the later-period ENSO response involves both a westward extension of Indo-Pacific circulation anomalies and a more central-Pacific-weighted convective structure, providing a large-scale dynamical setting through which northern SEA convection can be linked to AP rainfall variability.

4.2 Walker–Hadley circulation reorganization

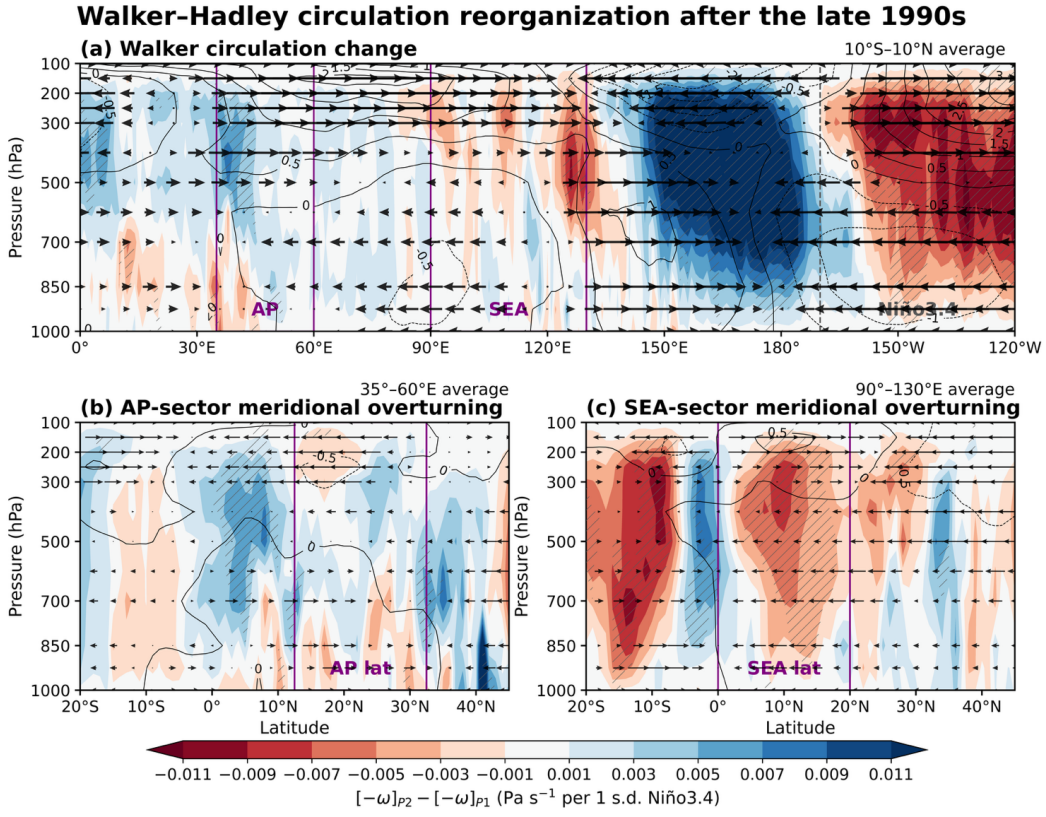

Figure 3: Walker–Hadley circulation reorganization after the late 1990s. P2–P1 differences in March–April regression onto the standardized Niño3.4 index for vertical motion and divergent circulation. Shading denotes -ω regression differences, so positive values indicate enhanced upward motion in P2 relative to P1 and

https://doi.org/10.5194/egusphere-2026-2784
Preprint. Discussion started: 1 June 2026

negative values indicate weakened ascent or enhanced subsidence. Vectors show the corresponding divergent circulation differences, with horizontal components given by $u\chi$ in (a) and $v\chi$ in (b,c), and vertical components given by scaled $-\omega$. Contours show the corresponding divergent-wind component differences: $u\chi$ in (a) and $v\chi$ in (b,c). (a) Longitude–pressure section averaged over 10°S–10°N, showing changes in the Walker circulation response. (b) Latitude–pressure section averaged over 35°–60°E, showing changes in the AP-sector meridional overturning response. (c) As in (b) but averaged over 90°–130°E for the SEA sector. Hatching indicates regions significant at the 95% confidence level. Purple boxes/vertical lines mark the AP, SEA, and Niño3.4 longitude or latitude ranges used in the analysis.

The circulation changes in Fig. 2 suggest that the SEA–AP rainfall seesaw is associated with an adjustment of tropical overturning. To examine this pathway, we diagnose P2–P1 differences in ENSO-regressed vertical motion and divergent circulation during March–April. Positive shading represents enhanced upward motion, expressed as $-\varpi$, in P2 relative to P1, whereas negative shading indicates weakened ascent or enhanced subsidence.

The longitude–pressure section averaged over 10°S–10°N shows a pronounced change in the Walker circulation response (Fig. 3a). Compared with P1, the later-period response is consistent with a more distinct Indo-Pacific double-cell overturning structure. This structure is dynamically consistent with the more central-Pacific-weighted, ENSO Modoki-like convective response identified in Fig. 2, as different ENSO heating patterns can alter the Walker circulation structure and Philippine Sea circulation response (Ashok et al., 2007; Nguyen-Le et al., 2024). For positive Niño3.4 anomalies, corresponding to El Niño conditions, the P2–P1 difference includes enhanced subsidence over SEA/Maritime Continent, a westward Indian Ocean–SEA Walker branch, and enhanced ascent over the western Indian Ocean/AP-side sector. The Pacific branch also shows a stronger contrast between the western/central Pacific and eastern Pacific. Thus, the later-period response reflects a reorganization of zonal overturning, rather than a uniform strengthening of the

https://doi.org/10.5194/egusphere-2026-2784
Preprint. Discussion started: 1 June 2026

Walker circulation. The corresponding P1 and P2 Walker-circulation regressions further confirm this shift in the vertical and zonal structure of ENSO-related overturning (Fig. S4).

The meridional sections show how this zonal overturning change projects onto the AP and SEA sectors. Over the AP sector, averaged over 35°–60°E, the P2–P1 difference shows a stronger vertical-motion response from low latitudes into the subtropical AP sector, with enhanced upward motion near the southern AP-side branch and adjacent subtropical latitudes (Fig. 3b). This suggests that the later-period ENSO response more effectively reaches the tropical–subtropical AP sector. Over the SEA sector, averaged over 90°–130°E, the response shows a stronger meridional contrast, with enhanced ascent south of the equator and enhanced subsidence or weakened ascent over parts of northern tropical SEA (Fig. 3c). The associated divergent circulation vectors indicate changes in upper- and lower-level meridional flow, consistent with an altered local Hadley-type circulation. The detailed P1 and P2 meridional vertical-motion regressions support this interpretation (Fig. S5). In P1, the AP-sector response is weak, whereas in P2 a clearer vertical-motion signal appears from low latitudes into the subtropical branch. The SEA sector also shows a stronger and more coherent tropical meridional structure in P2 than in P1. Similar results are obtained from the meridional mass streamfunction, which shows a stronger AP-sector overturning anomaly and a clearer SEA-sector meridional contrast after the late 1990s (Fig. S6).

These vertical-circulation diagnostics indicate that the post-1990s ENSO teleconnection change involves a coupled Walker–Hadley adjustment. The zonal overturning response develops a more distinct Indo-Pacific double-cell structure, consistent with the central-Pacific-weighted ENSO response, while regional meridional overturning changes become clearer over both SEA and the AP sector. This three-dimensional circulation adjustment provides a pathway through which ENSO-related tropical convection anomalies can connect SEA rainfall variability with AP rainfall variability.

https://doi.org/10.5194/egusphere-2026-2784
Preprint. Discussion started: 1 June 2026

4.3 Upper-level Rossby-type and thermal response

The Walker–Hadley changes described above suggest that the later-period ENSO response projects more clearly from the tropical Indo-Pacific toward the tropical–subtropical Asian sector. We next examine whether this reorganization is accompanied by changes in the off-equatorial upper-level circulation. Figure 4 shows P2–P1 differences in March–April regression onto the standardized Niño3.4 index for 200-hPa geopotential height Z_{200}, stationary wave activity flux (WAF), streamfunction, rotational wind, upper-tropospheric temperature, and Rossby wave source (RWS). These diagnostics are used to assess the Rossby-type and thermal components of the changed ENSO teleconnection.

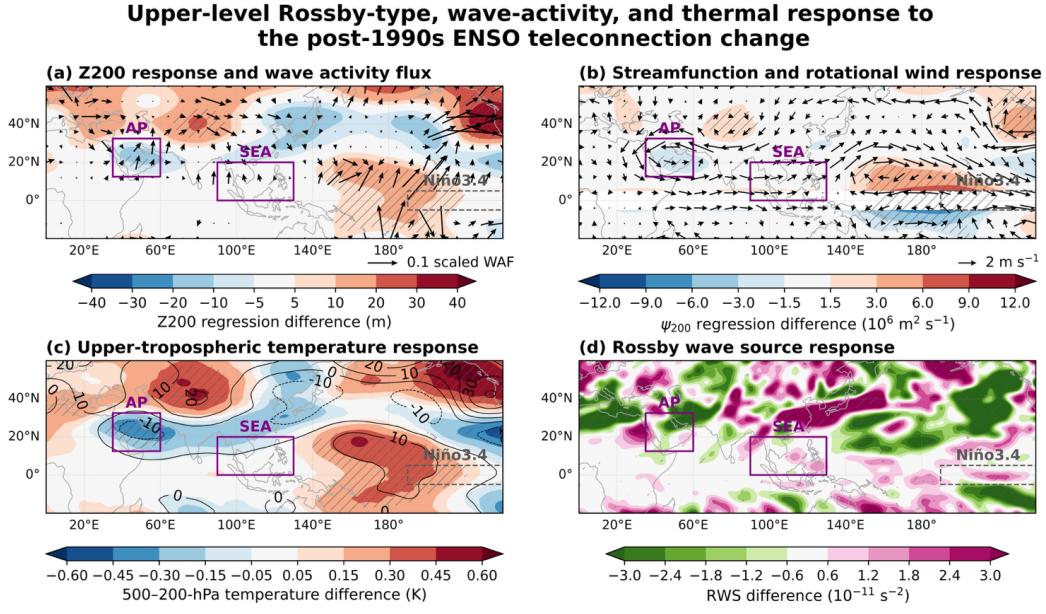

Figure 4: Upper-level Rossby-type, wave-activity, and thermal response to the post-1990s ENSO teleconnection change. Shading shows P2–P1 differences in March–April regression onto the standardized Niño3.4 index. (a) Difference in 200-hPa geopotential height Z200 regression, with vectors showing stationary wave activity flux (WAF). WAF vectors are scaled for display and interpreted qualitatively as indicators of the preferred wave-activity pathway; they are masked in the deep tropics. (b) Difference in 200-

https://doi.org/10.5194/egusphere-2026-2784
Preprint. Discussion started: 1 June 2026

hPa streamfunction ψ200 regression, with vectors showing the corresponding 200-hPa rotational wind response. (c) Difference in 500–200-hPa layer-mean temperature regression, with contours showing the Z200 response. (d) Difference in 200-hPa Rossby wave source (RWS). Stippling indicates bootstrap significance at the 95% confidence level. Purple boxes indicate the Arabian Peninsula (AP), northern Southeast Asia (SEA), and Niño3.4 regions.

The Z_{200} differences show a modified upper-level wave-like structure extending from the Indo-Pacific into the subtropical Asian sector (Fig. 4a). The associated WAF suggests a preferred stationary wave-activity pathway from the tropical–subtropical Indo-Pacific toward the subtropical circulation. This pattern is consistent with a later-period ENSO response that projects more effectively onto the subtropical Asian circulation. The 200-hPa streamfunction and rotational-wind differences provide a more direct view of the rotational component of this upper-level response (Fig. 4b). They show an altered off-equatorial circulation pattern over the Indo-Pacific–subtropical Asian sector, consistent with Rossby-type gyres associated with shifted ENSO-related tropical heating and upper-level divergent outflow. This pattern provides a plausible upper-level route through which the ENSO signal can be communicated from the tropical Pacific and Maritime Continent toward northern SEA and the AP sector.

The upper-tropospheric thermal response further supports this interpretation. The 500–200-hPa layer-mean temperature differences show a coherent thermal structure, with temperature anomalies broadly collocated with the Z_{200} response (Fig. 4c). This indicates that the later-period ENSO teleconnection includes not only a dynamical wave response but also an upper-tropospheric thermal adjustment. In particular, significant warming over the Tibetan Plateau/subtropical Asian sector and cooling over the AP–northern Indian Ocean indicate a changed upper-tropospheric thermal gradient. This gradient is dynamically consistent with the Z_{200} anomalies and may help support the northward projection of the AP-sector response.

https://doi.org/10.5194/egusphere-2026-2784
Preprint. Discussion started: 1 June 2026

The RWS provides a complementary diagnostic of the upper-level forcing environment (Fig. 4d). Its broad anomalies over the Indo-Pacific and subtropical belt are consistent with reorganized divergent-flow and vorticity fields. The time-varying index diagnostics provide additional support for the ENSO-related overturning pathway (Fig. S7). The Walker circulation index remains strongly coupled with Niño3.4 throughout the record, while its linkage with the AP vertical branch becomes more positive after the late 1990s and its linkage with the SEA vertical branch remains strongly negative. The weakening of the AP rainfall–SEA vertical-branch relationship after removing Niño3.4 further indicates that the regional overturning pathway is closely tied to ENSO forcing.

Overall, the upper-level diagnostics complement the Walker–Hadley analysis by showing that the later-period ENSO response is accompanied by off-equatorial rotational and thermal adjustments. These features provide a dynamically consistent upper-level component of the SEA–AP teleconnection pathway.

4.4 Idealized model simulations and sensitivity to the background state

The western North Pacific anticyclonic response to ENSO-related western Pacific convection anomalies is a well-established component of the Pacific–East Asian teleconnection and is already evident in the regression diagnostics. We therefore use the idealized model experiments to focus on the less direct western equatorial Indian Ocean–AP pathway. Identical heating is imposed over the western equatorial Indian Ocean under the P1 and P2 March–April basic states to test whether heating on the western side of the Indo-Pacific overturning system can generate an AP-sector circulation response, and whether that response depends on the background state (Fig. 5). The comparison is motivated by substantial post-1990s changes in the March–April mean circulation, including changes in the upper-level jet, OLR, low-level pressure and winds, and 200-hPa divergence (Fig. S8). These mean-state differences provide context for interpreting the later-period ENSO response, without being treated as direct analogues of the ENSO-regressed anomalies.

https://doi.org/10.5194/egusphere-2026-2784
Preprint. Discussion started: 1 June 2026

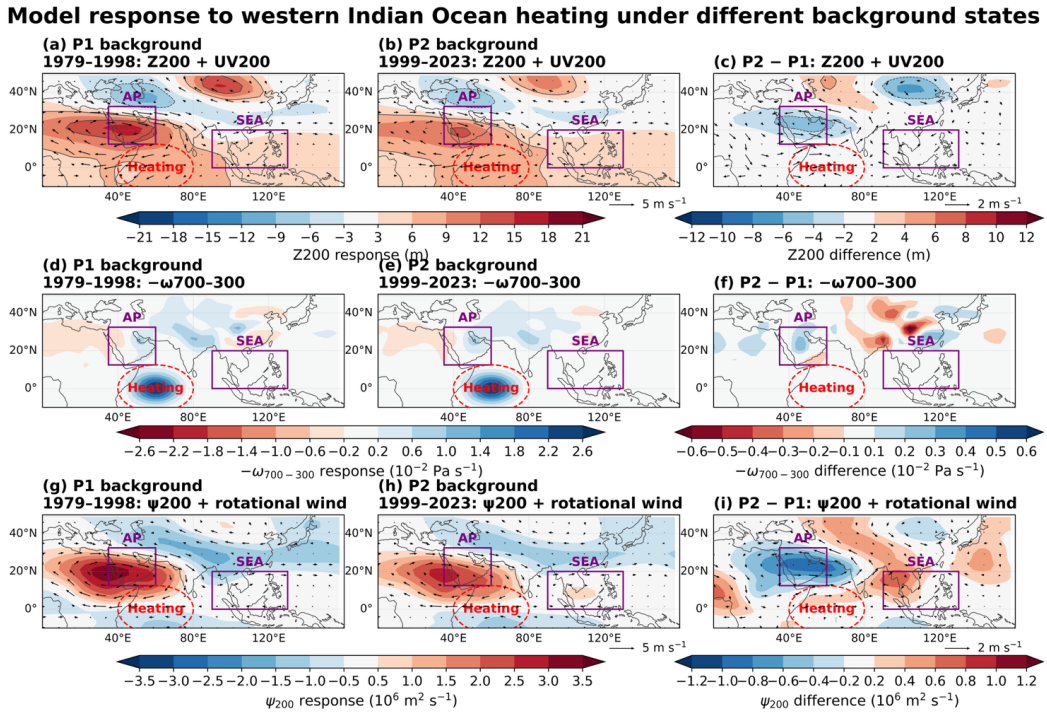

Figure 5: Idealized model response to western Indian Ocean heating under different March–April background states. Responses are calculated as the average over days 11–20. Columns show the response under the P1 background state (1979–1998), the response under the P2 background state (1999–2023), and their difference (P2–P1). Rows show the 200-hPa geopotential-height response with 200-hPa winds, the 700–300-hPa layer-mean -ω response, and the 200-hPa streamfunction response with 200-hPa rotational winds. Positive -ω indicates anomalous ascent. The red dashed ellipse marks the prescribed western equatorial Indian Ocean heating region, centered at 60°E, 0°N, and purple boxes indicate the Arabian Peninsula (AP) and northern Southeast Asia (SEA) regions.

The model produces an AP-sector response in both experiments, indicating that western equatorial Indian Ocean heating can excite upper-level and vertical-motion anomalies that extend toward the AP sector. This supports the physical plausibility of an AP response to heating anomalies associated with the reorganized Walker circulation. The P2–P1 differences further indicate sensitivity to the background state. Under the later-period basic state, negative Z_{200} and ψ_{200}

https://doi.org/10.5194/egusphere-2026-2784
Preprint. Discussion started: 1 June 2026

differences over the AP sector indicate a more cyclonic upper-level response, while positive -ω differences indicate stronger ascent or weaker subsidence relative to P1. Together, these features suggest that the P2 background state favors a stronger AP-sector vertical-motion response to western equatorial Indian Ocean heating.

These results indicate that western equatorial Indian Ocean heating can activate an AP-sector circulation response, with a more effective vertical-motion and upper-level circulation response under the later-period background state. Importantly, the P1 experiment shows that the background state alone does not determine whether an AP response is possible. The weaker observed SEA–AP teleconnection during P1 likely also reflects the weaker projection of ENSO-related convection and heating anomalies onto the western Indian Ocean/AP-side sector. In contrast, during P2, the observed ENSO-related convective response extends more clearly toward this region, allowing the heating pathway to operate more effectively. Thus, the observed circulation diagnostics provide the primary evidence for the post-1990s teleconnection change, while the idealized model experiments support the physical plausibility of the proposed heating-induced AP response. The background-state diagnostics further indicate that this response developed within a modified March–April mean circulation environment.

5. Discussion and conclusions

This study identifies a marked post-1990s strengthening of the March–April rainfall relationship between northern Southeast Asia and the Arabian Peninsula. During P1 (1979–1998), rainfall anomalies over the two regions were only weakly connected, whereas during P2 (1999–2023) they developed a clearer anti-phase relationship. Partial-correlation results indicate that this rainfall seesaw is primarily associated with ENSO rather than Indian Ocean basin-wide SST variability alone. This suggests that the SEA–AP rainfall linkage is not a stationary regional relationship, but an expression of a changing large-scale ENSO teleconnection.

https://doi.org/10.5194/egusphere-2026-2784
Preprint. Discussion started: 1 June 2026

The strengthened linkage is dynamically consistent with a reorganization of the Indo-Pacific circulation response to ENSO. In the later period, ENSO-related convection and low-level circulation anomalies project more clearly from the tropical Pacific and Maritime Continent toward northern SEA, the western North Pacific, the western equatorial Indian Ocean, and the AP sector. The western North Pacific anticyclonic component is consistent with the canonical Pacific–East Asian teleconnection framework (Wang et al., 2000; Xie et al., 2016; Li et al., 2017), in which ENSO-related western Pacific convection anomalies excite a lower-tropospheric anticyclonic response over the western North Pacific/Philippine Sea. In the present case, this canonical pathway becomes more pronounced after the late 1990s and is accompanied by a broader westward extension involving the western equatorial Indian Ocean and AP sector.

The later-period response also has a more central-Pacific-weighted, ENSO Modoki-like convective structure. Previous studies have shown that central-Pacific or ENSO Modoki-like forcing can alter the latitude and structure of the Walker circulation and modify the Philippine Sea circulation response (Ashok et al., 2007; Nguyen-Thanh et al., 2023; Nguyen-Le et al., 2024). This provides a useful dynamical context for the more distinct Indo-Pacific double-cell Walker response diagnosed here. For El Niño conditions, enhanced descent over SEA/Maritime Continent and ascent over the western equatorial Indian Ocean/AP-side sector provide a plausible overturning pathway for opposite rainfall anomalies between the two regions. Vertical-circulation diagnostics further show clearer meridional overturning anomalies over the SEA and AP sectors, while the upper-level diagnostics indicate accompanying off-equatorial Rossby-type and thermal adjustments. Together, these features suggest that the post-1990s rainfall seesaw reflects a three-dimensional reorganization of ENSO-related tropical overturning and upper-level circulation, rather than an isolated regional rainfall change.

The idealized DREAM experiments provide additional support for this interpretation. Under identical western equatorial Indian Ocean heating, the model produces an AP-sector response under

https://doi.org/10.5194/egusphere-2026-2784
Preprint. Discussion started: 1 June 2026

both P1 and P2 basic states, indicating that heating on the western side of the Indo-Pacific overturning system can excite circulation anomalies relevant to AP rainfall. The P2–P1 differences further show that the later-period basic state modifies the forced response, including the upper-level geopotential-height and streamfunction patterns and the AP-sector vertical-motion response. These results suggest that the background state can influence the structure and efficiency of the SEA–AP teleconnection. At the same time, the P1 experiment shows that background-state sensitivity alone cannot explain the observed transition. The weaker observed SEA–AP linkage during P1 likely also reflects the weaker projection of ENSO-related convection and heating anomalies onto the western equatorial Indian Ocean/AP-side sector during that period.

Figure 6 summarizes the proposed mechanism. During the earlier period, ENSO-related anomalies are more Pacific-centered and remain more closely tied to the tropical Pacific–Maritime Continent/northern SEA sector, with only weak projection toward the AP. After the late 1990s, the response becomes more central-Pacific-weighted and extends farther westward and northwestward, strengthening the connection among northern SEA, the western equatorial Indian Ocean, and the AP sector through coupled Walker–Hadley overturning and upper-level circulation adjustment. Overall, the results suggest that the SEA–AP rainfall seesaw reflects a nonstationary ENSO teleconnection pathway, in which the westward extension of tropical heating anomalies, a more distinct double-cell Walker response, regional Walker–Hadley coupling, and off-equatorial upper-level adjustment jointly shape spring rainfall variability across Southeast and West Asia.

This nonstationarity also has implications for seasonal prediction and hydroclimate risk assessment. Prediction systems and statistical models trained over long historical periods may underestimate the recent strength of the SEA–AP rainfall linkage, particularly if the ENSO–rainfall relationship changes across decades. The post-1990s anti-phase relationship suggests that ENSO information may provide greater predictive value for AP spring rainfall variability than indicated by earlier-period relationships alone, consistent with previous studies highlighting the importance of

https://doi.org/10.5194/egusphere-2026-2784
Preprint. Discussion started: 1 June 2026

529 large-scale climate drivers for seasonal rainfall prediction over the region (Almazroui et al., 2022).
530 At the same time, the dependence of this linkage on the evolving Indo-Pacific background state
531 implies that prediction skill may itself be nonstationary.

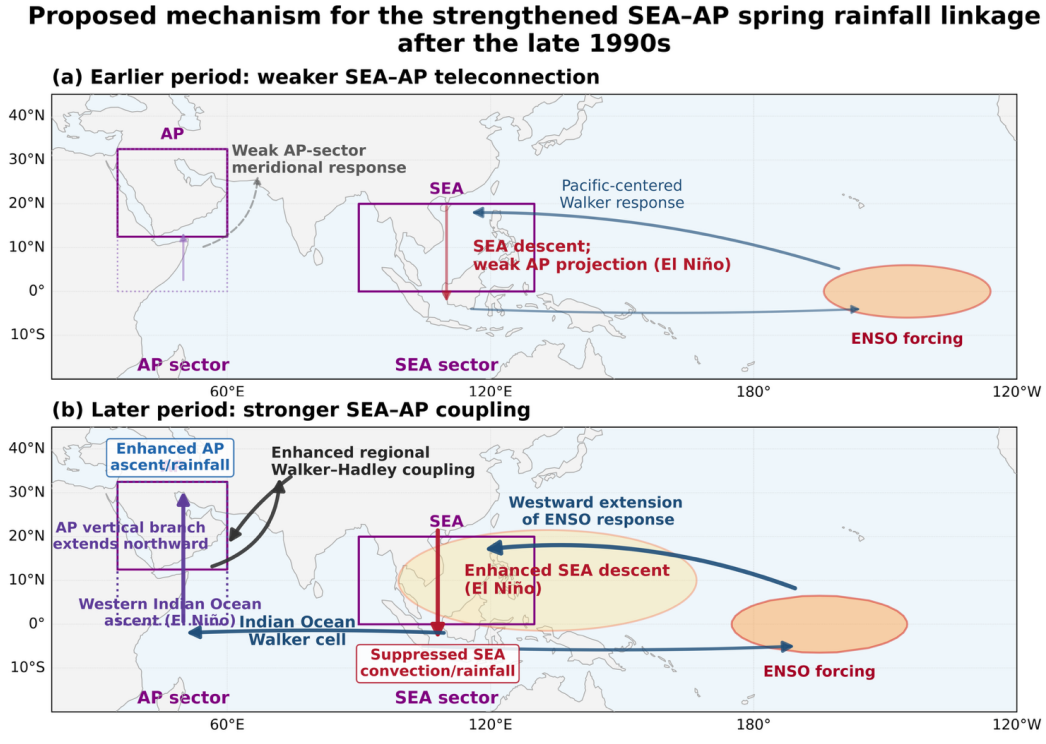

532

533 **Figure 6:** Schematic diagram of the proposed post-1990s ENSO teleconnection pathway linking northern
534 Southeast Asian and Arabian Peninsula spring rainfall. The schematic illustrates the response to El Niño
535 conditions; opposite-sign circulation and rainfall anomalies are expected during La Niña. During the earlier
536 period, ENSO-related circulation anomalies are more Pacific-centered and remain mainly tied to the tropical
537 Pacific–Maritime Continent/northern SEA sector, with only weak projection toward the Arabian Peninsula
538 (AP) and a limited AP-sector meridional response. After the late 1990s, the ENSO-related response becomes
539 more central-Pacific-weighted and extends farther westward and northwestward toward the western equatorial
540 Indian Ocean and subtropical AP sector, strengthening the dynamical connection between northern SEA and
541 the AP. This later-period pathway is characterized by a more distinct Indo-Pacific double-cell Walker
542 response, including enhanced SEA/Maritime Continent descent, a westward Indian Ocean–SEA Walker

https://doi.org/10.5194/egusphere-2026-2784
Preprint. Discussion started: 1 June 2026

543 branch, and western equatorial Indian Ocean ascent. The AP vertical branch becomes stronger and extends
544 farther northward, while Walker–Hadley coupling and upper-level Rossby-type/thermal adjustment provide
545 additional pathways for communicating the ENSO signal into the subtropical Asian sector. Background-state
546 changes may influence the efficiency of this pathway, supporting a stronger anti-phase spring rainfall
547 relationship between SEA and the AP.

548 Several caveats should be noted. First, although the DREAM experiments provide useful
549 dynamical support, the observational diagnostics and idealized model experiments are not sufficient
550 to fully isolate causality. Future work using state-of-the-art climate models will be useful for further
551 testing the proposed mechanisms. Second, although the post-1990s strengthening of the SEA–AP
552 rainfall linkage is robust across different moving-window lengths and rainfall datasets, the
553 observational record remains relatively short for diagnosing decadal changes in this linkage. Third,
554 AP and SEA rainfall are influenced by multiple processes, including subtropical westerlies, regional
555 moisture transport, transient disturbances, land–atmosphere interactions, and local convection.
556 ENSO provides an important large-scale control, but it is unlikely to be the only driver of spring
557 rainfall variability (Almazroui, 2023; Horan et al., 2023). The roles of non-ENSO factors therefore
558 deserve further investigation.

559 **Code Availability** Detailed information on the DREAM model is available at
560 https://github.com/dream-gcm, and the model source code can be obtained from the developers upon
561 reasonable request. The codes used for data analysis and visualization are available from the author
562 upon reasonable request.

563 **Data Availability** The datasets used in this study are publicly available from the following sources:
564 ERA5 (ECMWF; https://www.ecmwf.int/en/forecasts/dataset/ecmwf-reanalysis-v5); HadISST (UK
565 Met Office Hadley Centre; https://www.metoffice.gov.uk/hadobs/hadisst); OLR CDR (NOAA
566 NCEI; https://www.ncei.noaa.gov/products/climate-data-records/outgoing-longwave-radiation-
567 monthly); CMAP (NOAA Physical Sciences Laboratory;

https://doi.org/10.5194/egusphere-2026-2784
Preprint. Discussion started: 1 June 2026

https://psl.noaa.gov/data/gridded/data.cmap.html); and GPCP (NASA; https://www.ncei.noaa.gov/data/global-precipitation-climatology-project-gpcp-monthly).

Author contributions The author conceived the study, performed the analysis, and wrote the manuscript.

Competing interests The author declares no conflict of interest..

Acknowledgments The author gratefully acknowledges Prof. Nicholas M. J. Hall and Dr. Stephanie Leroux for their invaluable guidance and assistance with the DREAM model.

Financial support This research did not receive any specific grant from funding agencies in the public, commercial, or not-for-profit sectors.

References

Adler, R. F., Huffman, G. J., Chang, A., Ferraro, R., Xie, P.-P., Janowiak, J., Rudolf, B., Schneider, U., Curtis, S., Bolvin, D., Gruber, A., Susskind, J., Arkin, P., and Nelkin, E.: The Version-2 Global Precipitation Climatology Project (GPCP) Monthly Precipitation Analysis (1979–Present), J. Hydrometeor, 4, 1147–1167, https://doi.org/10.1175/1525-7541(2003)004%3C1147:TVGPCP%3E2.0.CO;2, 2003.

Alexander, M. A., Bladé, I., Newman, M., Lanzante, J. R., Lau, N.-C., and Scott, J. D.: The Atmospheric Bridge: The Influence of ENSO Teleconnections on Air–Sea Interaction over the Global Oceans, J. Climate, 15, 2205–2231, https://doi.org/10.1175/1520-0442(2002)015%3C2205:TABTIO%3E2.0.CO;2, 2002.

Almazroui, M.: The Influence of the Madden–Julian Oscillation on the Wet Season Rainfall over Saudi Arabia, Earth Syst Environ, 7, 1–14, https://doi.org/10.1007/s41748-022-00334-w, 2023.

https://doi.org/10.5194/egusphere-2026-2784
Preprint. Discussion started: 1 June 2026

589 Almazroui, M., Rashid, I. U., Saeed, S., and Islam, M. N.: ENSO influence on summer temperature
590 over Arabian Peninsula: role of mid-latitude circulation, Clim Dyn, 53, 5047–5062,
591 https://doi.org/10.1007/s00382-019-04848-4, 2019.

592 Almazroui, M., Khalid, S., Kamil, S., Ismail, M., Islam, M. N., Saeed, S., Abid, M. A., Ehsan, M. A.,
593 and Hantoush, A. S.: Skill assessment of Saudi-KAU and C3S models in prediction of spring season
594 rainfall over the Arabian Peninsula, Atmospheric Research, 280, 106461,
595 https://doi.org/10.1016/j.atmosres.2022.106461, 2022.

596 Ashok, K., Behera, S. K., Rao, S. A., Weng, H., and Yamagata, T.: El Niño Modoki and its possible
597 teleconnection, J. Geophys. Res., 112, 2006JC003798, https://doi.org/10.1029/2006JC003798, 2007.

598 Barlow, M., Zaitchik, B., Paz, S., Black, E., Evans, J., and Hoell, A.: A Review of Drought in the
599 Middle East and Southwest Asia, Journal of Climate, 29, 8547–8574, https://doi.org/10.1175/JCLI-
600 D-13-00692.1, 2016.

601 Bretherton, C. S., Widmann, M., Dymnikov, V. P., Wallace, J. M., and Bladé, I.: The Effective
602 Number of Spatial Degrees of Freedom of a Time-Varying Field, J. Climate, 12, 1990–2009,
603 https://doi.org/10.1175/1520-0442(1999)012%3C1990:TENOSD%3E2.0.CO;2, 1999.

604 Cai, W., Borlace, S., Lengaigne, M., Van Rensch, P., Collins, M., Vecchi, G., Timmermann, A.,
605 Santoso, A., McPhaden, M. J., Wu, L., England, M. H., Wang, G., Guilyardi, E., and Jin, F.-F.:
606 Increasing frequency of extreme El Niño events due to greenhouse warming, Nature Clim Change, 4,
607 111–116, https://doi.org/10.1038/nclimate2100, 2014.

608 Chang, C.-P., Wang, Z., McBride, J., and Liu, C.-H.: Annual Cycle of Southeast Asia—Maritime
609 Continent Rainfall and the Asymmetric Monsoon Transition, Journal of Climate, 18, 287–301,
610 https://doi.org/10.1175/JCLI-3257.1, 2005.

https://doi.org/10.5194/egusphere-2026-2784
Preprint. Discussion started: 1 June 2026

611 Deser, C., Phillips, A. S., and Hurrell, J. W.: Pacific Interdecadal Climate Variability: Linkages
612 between the Tropics and the North Pacific during Boreal Winter since 1900, J. Climate, 17, 3109–
613 3124, https://doi.org/10.1175/1520-0442(2004)017%3C3109:PICVLB%3E2.0.CO;2, 2004.

614 Dong, L. and McPhaden, M. J.: Why Has the Relationship between Indian and Pacific Ocean
615 Decadal Variability Changed in Recent Decades?, Journal of Climate, 30, 1971–1983,
616 https://doi.org/10.1175/JCLI-D-16-0313.1, 2017.

617 Hall, N. M. J.: A Simple GCM Based on Dry Dynamics and Constant Forcing, J. Atmos. Sci., 57,
618 1557–1572, https://doi.org/10.1175/1520-0469(2000)057%3C1557:ASGBOD%3E2.0.CO;2, 2000.

619 Hall, N. M. J. and Derome, J.: Transience, Nonlinearity, and Eddy Feedback in the Remote Response
620 to El Niño, J. Atmos. Sci., 57, 3992–4007, https://doi.org/10.1175/1520-
621 0469(2001)058%3C3992:TNAEFI%3E2.0.CO;2, 2000.

622 Hall, N. M. J. and Leroux, S.: Dream user manual v8.4, https://doi.org/10.5281/ZENODO.8414525,
623 2023.

624 Hersbach, H., Bell, B., Berrisford, P., Hirahara, S., Horányi, A., Muñoz-Sabater, J., Nicolas, J.,
625 Peubey, C., Radu, R., Schepers, D., Simmons, A., Soci, C., Abdalla, S., Abellan, X., Balsamo, G.,
626 Bechtold, P., Biavati, G., Bidlot, J., Bonavita, M., De Chiara, G., Dahlgren, P., Dee, D.,
627 Diamantakis, M., Dragani, R., Flemming, J., Forbes, R., Fuentes, M., Geer, A., Haimberger, L.,
628 Healy, S., Hogan, R. J., Hólm, E., Janisková, M., Keeley, S., Laloyaux, P., Lopez, P., Lupu, C.,
629 Radnoti, G., De Rosnay, P., Rozum, I., Vamborg, F., Villaume, S., and Thépaut, J.: The ERA5
630 global reanalysis, Quart J Royal Meteoro Soc, 146, 1999–2049, https://doi.org/10.1002/qj.3803,
631 2020.

632 Horan, M. F., Batibeniz, F., Kucharski, F., Almazroui, M., Abid, M. A., Fu, J. S., and Ashfaq, M.:
633 Moisture sources for precipitation variability over the Arabian Peninsula, Clim Dyn, 61, 4793–4807,
634 https://doi.org/10.1007/s00382-023-06762-2, 2023.

https://doi.org/10.5194/egusphere-2026-2784
Preprint. Discussion started: 1 June 2026

635 Hoskins, B. J. and Karoly, D. J.: The Steady Linear Response of a Spherical Atmosphere to Thermal
636 and Orographic Forcing, J. Atmos. Sci., 38, 1179–1196, https://doi.org/10.1175/1520-
637 0469(1981)038%3C1179:TSLROA%3E2.0.CO;2, 1981.

638 Hu, Z.-Z., Kumar, A., Ren, H.-L., Wang, H., L'Heureux, M., and Jin, F.-F.: Weakened Interannual
639 Variability in the Tropical Pacific Ocean since 2000, Journal of Climate, 26, 2601–2613,
640 https://doi.org/10.1175/JCLI-D-12-00265.1, 2013.

641 Hu, Z.-Z., Kumar, A., Huang, B., Zhu, J., L'Heureux, M., McPhaden, M. J., and Yu, J.-Y.: The
642 Interdecadal Shift of ENSO Properties in 1999/2000: A Review, Journal of Climate, 33, 4441–4462,
643 https://doi.org/10.1175/JCLI-D-19-0316.1, 2020.

644 Juneng, L. and Tangang, F. T.: Evolution of ENSO-related rainfall anomalies in Southeast Asia
645 region and its relationship with atmosphere–ocean variations in Indo-Pacific sector, Climate
646 Dynamics, 25, 337–350, https://doi.org/10.1007/s00382-005-0031-6, 2005.

647 Kang, I.-S., Rashid, I. U., Kucharski, F., Almazroui, M., and Alkhalaf, A. K.: Multidecadal Changes
648 in the Relationship between ENSO and Wet-Season Precipitation in the Arabian Peninsula, Journal
649 of Climate, 28, 4743–4752, https://doi.org/10.1175/JCLI-D-14-00388.1, 2015.

650 Kiguchi, M., Matsumoto, J., Kanae, S., and Oki, T.: Pre-Monsoon Rain and Its Relationship with
651 Monsoon Onset over the Indochina Peninsula, Front. Earth Sci., 4,
652 https://doi.org/10.3389/feart.2016.00042, 2016.

653 Lee, H.-T., Gruber, A., Ellingson, R. G., and Laszlo, I.: Development of the HIRS Outgoing
654 Longwave Radiation Climate Dataset, Journal of Atmospheric and Oceanic Technology, 24, 2029–
655 2047, https://doi.org/10.1175/2007JTECHA989.1, 2007.

656 Leroux, S. and Hall, N.: Tutorial notebooks to get started with the DREAM model (v1.1), ,
657 https://doi.org/10.5281/ZENODO.16079415, 2025.

https://doi.org/10.5194/egusphere-2026-2784
Preprint. Discussion started: 1 June 2026

658 Li, T., Wang, B., Wu, B., Zhou, T., Chang, C.-P., and Zhang, R.: Theories on formation of an
659 anomalous anticyclone in western North Pacific during El Niño: A review, J Meteorol Res, 31, 987–
660 1006, https://doi.org/10.1007/s13351-017-7147-6, 2017.

661 Lin, H., Derome, J., and Brunet, G.: The Nonlinear Transient Atmospheric Response to Tropical
662 Forcing, Journal of Climate, 20, 5642–5665, https://doi.org/10.1175/2007JCLI1383.1, 2007.

663 LinHo, L. H., Huang, X., and Lau, N.-C.: Winter-to-Spring Transition in East Asia: A Planetary-
664 Scale Perspective of the South China Spring Rain Onset, Journal of Climate, 21, 3081–3096,
665 https://doi.org/10.1175/2007JCLI1611.1, 2008.

666 Lübbecke, J. F. and McPhaden, M. J.: Assessing the Twenty-First-Century Shift in ENSO Variability
667 in Terms of the Bjerknes Stability Index*, Journal of Climate, 27, 2577–2587,
668 https://doi.org/10.1175/JCLI-D-13-00438.1, 2014.

669 McPhaden, M. J., Zebiak, S. E., and Glantz, M. H.: ENSO as an Integrating Concept in Earth
670 Science, Science, 314, 1740–1745, https://doi.org/10.1126/science.1132588, 2006.

671 Nguyen–Le, D.: Projected ENSO teleconnection on the Southeast Asian climate under global
672 warming, Environ. Res. Lett., 19, 014001, https://doi.org/10.1088/1748-9326/ad0d3e, 2024.

673 Nguyen-Le, D., Ngo-Duc, T., and Matsumoto, J.: The teleconnection of the two types of ENSO and
674 Indian Ocean Dipole on Southeast Asian autumn rainfall anomalies, Clim Dyn, 62, 1–23,
675 https://doi.org/10.1007/s00382-024-07163-9, 2024.

676 Nguyen-Thanh, H., Ngo-Duc, T., and Herrmann, M.: The distinct impacts of the two types of ENSO
677 on rainfall variability over Southeast Asia, Clim Dyn, 61, 2155–2172,
678 https://doi.org/10.1007/s00382-023-06673-2, 2023.

https://doi.org/10.5194/egusphere-2026-2784
Preprint. Discussion started: 1 June 2026

679 Peel, M. C., Finlayson, B. L., and McMahon, T. A.: Updated world map of the Köppen-Geiger
680 climate classification, Hydrol. Earth Syst. Sci., 11, 1633–1644, https://doi.org/10.5194/hess-11-
681 1633-2007, 2007.

682 Power, S., Casey, T., Folland, C., Colman, A., and Mehta, V.: Inter-decadal modulation of the
683 impact of ENSO on Australia, Climate Dynamics, 15, 319–324,
684 https://doi.org/10.1007/s003820050284, 1999.

685 Räsänen, T. A., Lindgren, V., Guillaume, J. H. A., Buckley, B. M., and Kummu, M.: On the spatial
686 and temporal variability of ENSO precipitation and drought teleconnection in mainland Southeast
687 Asia, Clim. Past, 12, 1889–1905, https://doi.org/10.5194/cp-12-1889-2016, 2016.

688 Rasmusson, E. M. and Carpenter, T. H.: Variations in Tropical Sea Surface Temperature and Surface
689 Wind Fields Associated with the Southern Oscillation/El Niño, Mon. Wea. Rev., 110, 354–384,
690 https://doi.org/10.1175/1520-0493(1982)110%3C0354:VITSST%3E2.0.CO;2, 1982.

691 Rayner, N. A., Parker, D. E., Horton, E. B., Folland, C. K., Alexander, L. V., Rowell, D. P., Kent, E.
692 C., and Kaplan, A.: Global analyses of sea surface temperature, sea ice, and night marine air
693 temperature since the late nineteenth century, J. Geophys. Res., 108, 2002JD002670,
694 https://doi.org/10.1029/2002JD002670, 2003.

695 Rodrigues, R. R., Subramanian, A., Zanna, L., and Berner, J.: ENSO Bimodality and Extremes,
696 Geophysical Research Letters, 46, 4883–4893, https://doi.org/10.1029/2019GL082270, 2019.

697 Rodwell, M. J. and Hoskins, B. J.: Monsoons and the dynamics of deserts, Quart J Royal Meteoro
698 Soc, 122, 1385–1404, https://doi.org/10.1002/qj.49712253408, 1996.

699 Sardeshmukh, P. D. and Hoskins, B. J.: The Generation of Global Rotational Flow by Steady
700 Idealized Tropical Divergence, J. Atmos. Sci., 45, 1228–1251, https://doi.org/10.1175/1520-
701 0469(1988)045%3C1228:TGOGRF%3E2.0.CO;2, 1988.

https://doi.org/10.5194/egusphere-2026-2784
Preprint. Discussion started: 1 June 2026

Storch, H. V. and Zwiers, F. W.: Statistical Analysis in Climate Research:, 1st ed., Cambridge University Press, https://doi.org/10.1017/CBO9780511612336, 1999.

Takaya, K. and Nakamura, H.: A Formulation of a Phase-Independent Wave-Activity Flux for Stationary and Migratory Quasigeostrophic Eddies on a Zonally Varying Basic Flow, J. Atmos. Sci., 58, 608–627, https://doi.org/10.1175/1520-0469(2001)058%3C0608:AFOAPI%3E2.0.CO;2, 2001.

Trenberth, K. E., Caron, J. M., Stepaniak, D. P., and Worley, S.: Evolution of El Niño–Southern Oscillation and global atmospheric surface temperatures, J.-Geophys.-Res., 107, https://doi.org/10.1029/2000JD000298, 2002.

Vecchi, G. A., Soden, B. J., Wittenberg, A. T., Held, I. M., Leetmaa, A., and Harrison, M. J.: Weakening of tropical Pacific atmospheric circulation due to anthropogenic forcing, Nature, 441, 73–76, https://doi.org/10.1038/nature04744, 2006.

Wang, B., Wu, R., and Fu, X.: Pacific–East Asian Teleconnection: How Does ENSO Affect East Asian Climate?, J. Climate, 13, 1517–1536, https://doi.org/10.1175/1520-0442(2000)013%3C1517:PEATHD%3E2.0.CO;2, 2000.

Wang, B., Liu, J., Kim, H.-J., Webster, P. J., Yim, S.-Y., and Xiang, B.: Northern Hemisphere summer monsoon intensified by mega-El Niño/southern oscillation and Atlantic multidecadal oscillation, Proc. Natl. Acad. Sci. U.S.A., 110, 5347–5352, https://doi.org/10.1073/pnas.1219405110, 2013.

Wang, B., Luo, X., and Liu, J.: How Robust is the Asian Precipitation–ENSO Relationship during the Industrial Warming Period (1901–2017)?, Journal of Climate, 33, 2779–2792, https://doi.org/10.1175/JCLI-D-19-0630.1, 2020.

Whittaker, J.: Graphical models in applied multivariate statistics, paperback ed., 1. publ., Wiley, Chichester, 448 pp., 2008.

https://doi.org/10.5194/egusphere-2026-2784
Preprint. Discussion started: 1 June 2026

725 Xie, P. and Arkin, P. A.: Global Precipitation: A 17-Year Monthly Analysis Based on Gauge
726 Observations, Satellite Estimates, and Numerical Model Outputs, Bull. Amer. Meteor. Soc., 78,
727 2539–2558, https://doi.org/10.1175/1520-0477(1997)078%3C2539:GPAYMA%3E2.0.CO;2, 1997.

728 Xie, S.-P., Kosaka, Y., Du, Y., Hu, K., Chowdary, J. S., and Huang, G.: Indo-western Pacific ocean
729 capacitor and coherent climate anomalies in post-ENSO summer: A review, Adv. Atmos. Sci., 33,
730 411–432, https://doi.org/10.1007/s00376-015-5192-6, 2016.

731 Yang, J., Liu, Q., Xie, S., Liu, Z., and Wu, L.: Impact of the Indian Ocean SST basin mode on the
732 Asian summer monsoon, Geophysical Research Letters, 34, 2006GL028571,
733 https://doi.org/10.1029/2006GL028571, 2007.

734 Yang, J., Liu, Q., Liu, Z., Wu, L., and Huang, F.: Basin mode of Indian Ocean sea surface
735 temperature and Northern Hemisphere circumglobal teleconnection, Geophysical Research Letters,
736 36, 2009GL039559, https://doi.org/10.1029/2009GL039559, 2009.

737 Yeh, S.-W., Kug, J.-S., Dewitte, B., Kwon, M.-H., Kirtman, B. P., and Jin, F.-F.: El Niño in a
738 changing climate, Nature, 461, 511–514, https://doi.org/10.1038/nature08316, 2009.

739 Zheng, Y. and Hoteit, I.: Asymmetric Impacts of Indian Ocean Dipole on Summer Climate Over
740 Arabian Peninsula, Geophysical Research Letters, 52, e2025GL118195,
741 https://doi.org/10.1029/2025GL118195, 2025.